Integrating an Ultramicroelectrode in an AFM Cantilever: Combined Technology for Enhanced Information

ARTICLE *in* ANALYTICAL CHEMISTRY · JULY 2001

Impact Factor: 5.64 · DOI: 10.1021/ac001099v · Source: PubMed

6 AUTHORS, INCLUDING:

Christine Kranz
Universität Ulm
130 PUBLICATIONS **2,448** CITATIONS
SEE PROFILE

Boris Mizaikoff
Universität Ulm
310 PUBLICATIONS **4,799** CITATIONS
SEE PROFILE

Alois Lugstein
TU Wien
129 PUBLICATIONS **1,726** CITATIONS
SEE PROFILE

Anal. Chem. **2001,** *73,* 2491−2500

Integrating an Ultramicroelectrode in an AFM Cantilever: Combined Technology for Enhanced Information

Christine Kranz,*,† Gernot Friedbacher, and Boris Mizaikoff†

Institute of Analytical Chemistry, Vienna University of Technology, Getreidemarkt 9/151, A-1060 Wien, Austria

Alois Lugstein, JÜrgen Smoliner, and Emmerich Bertagnolli

Institut für Festkörperelektronik & Mikrostrukturzentrum der TU-Wien, Floragasse 7, A-1040 Wien, Austria

We present a novel approach to develop and process a microelectrode integrated in a standard AFM tip. The presented fabrication process allows the integration of an electroactive area at an exactly defined distance above of the end of a scanning probe tip and the subsequent remodeling and sharpening of the original AFM tip using a focused ion beam (FIB) technique (See ref 1 for patent information). Thus, the functionality of scanning electrochemical microscopy (SECM) can be integrated into any standard atomic force microscope (AFM). With the demonstrated approach, a precisely defined and constant distance between the microelectrode and the sample surface can be obtained, alternatively to the indirect determination of this distance usually applied in SECM experiments. Hence, a complete separation of the topographical information and the electrochemical signal is possible. The presented technique is a significant step toward electrochemical imaging with submicrometer electrodes as demonstrated by the development of the first integrated frame submicroelectrode.

Miniaturization of electrodes and electrochemical transducers by microfabrication processes is one of the fundamentals in modern electroanalytical chemistry.[2] Mainly thin-film and microlithographic techniques originating from the field of microelectronics are used to produce geometrically well-defined planar microelectrodes and microelectrode arrays. Although bulk micromachining is commonly used for 3-dimensional structuring of silicon, for example cantilever probe fabrication, up to now, this technique has barely found application in the development of 3-dimensional electrochemical microsystems.[3]

Laterally resolved information on a submicrometer scale was added to electroanalytical chemistry with the invention of scanning electrochemical microscopy (SECM).[4,5] This analytical method provides spatially resolved information on interface processes, which can be obtained by the use of all common electrochemical methods, such as amperometry, potentiometry, or cyclic voltammetry. The electrodes are usually manufactured by melting a metal wire in glass and subsequent grinding and polishing to produce a disc-shaped microelectrode,[6−8] which is subsequently deployed as scanning probe in SECM. The changes of the diffusion-limited Faraday current at the microelectrode due to hemispherical diffusion of a redox mediator, are recorded while scanning in constant height in the *x-y* plane within a distance of a few electrode radii above the sample surface. The current response as a function of the microelectrode position is mainly influenced by the morphology and the reactivity of the investigated surface and the distance between the microelectrode and the sample. Numerical solutions of Fick's diffusion equations allow the quantification of experimental SECM data;[9] however, a precise knowledge of the tip-to-sample distance is a prerequisite. This distance is determined by fitting the experimental current/distance curves to theoretical data, which are established for well-known tip geometries.[10,11] Because the constant-height imaging mode with a fitted tip-to-sample distance is the common procedure, disc-shaped micro-

* Email: christine.kranz@chemistry.gatech.edu.

† Present address: School of Chemistry and Biochemistry, Georgia Institute of Technology, Atlanta, GA 30332-0400.

(1) (a) Patent pending, A 1011/2000 G01N, June 09, **2000**. (b) Patent pending, A 1012/2000 G01N, June 09, **2000**.

(2) Montenegro, M. I.; Queiros, A. A.; Daschbach, J. D. *Microelctrodes: Theory and Applications*; Kluwer: Dordrecht, The Netherlands, 1990.

(3) Hoogerwerf, A.; Wise, K. D. *IEEE Trans. Biomed. Engin.* **1994**, *41*, 1136.

(4) Liu, H. Y.; Fan, F.-R. F.; Lin, C. W.; Bard, A. J. *J. Am. Chem. Soc.* **1986**, *108*, 3838.

(5) (a) Engstrom, R. C.; Weber, M.; Wunder, D. J.; Burgess, R.; Winquist, S. *Anal. Chem.* **1986**, *58*, 844. (b) Engstrom, R. C.; Meany, T.; Tople, R.; Wightman, R. M. *Anal. Chem.* **1987**, *59*, 2005.

(6) Baer, C. D.; Stone, N. J.; Sweigart, D. A. *Anal. Chem.* **1988**, *60*, 188.

(7) (a) Wightman, R. M.; Wipf, D. O. In *Electroanalytical Chemistry*; Bard, A. J., Ed.; Marcel Dekker: New York, 1988; Vol. 15, p 328. (b) Bard, A. J.; Fan, F.-R. F.; Mirkin, M. V. In *Electroanalytical Chemistry*; Bard, A. J., Ed.; Marcel Dekker: New York, 1994; Vol. 18, p 243.

(8) Heinze, J. *Angew. Chem., Int. Ed. Engl.* **1993**, *32*, 1265.

(9) (a) Bard, A. J.; Fan, F.-R. F.; Mirkin, M. V. In *Physical Electrochemistry: Principles, Methods and Applications*; Rubenstein, I., Ed.; Marcel Dekker: New York, 1995, p 209. (b) Bard, A. J.; Fan, F.-R. F.; Pierce, D. T.; Unwin, P. R.; Wipf, D. O.; Zhou, F. *Science* **1991**, *254*, 68. (c) Mirkin, M. V. *Anal. Chem.* **1996**, *5*, A177.

(10) (a) Kwak, J.; Bard, A. J. *Anal. Chem.* **1989**, *61* 1221. (b) Mirkin, M. V.; Fan, F.-R. F.; Bard, A. J. *J. Electroanal. Chem.* **1992**, *328*, 47.

(11) Amphlett, J. L.; Denuault, G. *J. Phys. Chem. B* **1998**, *102*, 9946.

10.1021/ac001099v CCC: $20.00
Published on Web 04/26/2001

electrodes with diameters ranging from 2 to 25 μm are usually applied in SECM experiments.

Any further progress in information quantification and qualification needs to address (i) submicrometer- to nanometer-sized electrodes (nanoelectrodes) for improved lateral resolution, (ii) the integration of current independent height information, and (iii) the precise knowledge of the distance between the electrode tip and the sample surface. Consequently, the combination of SECM with other scanning probe techniques, such as scanning tunneling microscopy (STM), atomic force microscopy (AFM), scanning nearfield optical microscopy (SNOM), etc., is of particular interest in order to overcome the current limitations and to obtain complementary surface information.

Although several groups have been exploring methods to fabricate nanoelectrodes either by electrochemical etching[12,13] or by laser-based micropipet pulling of metal microwires in glass,[14] only a few results have been published using such small electrodes in a conventional SECM experiment.[15] The main reason is the difficulty in scanning with submicrometer electrodes because of a working distance in the nanometer range. Thus, "tip crashes" may result when insufficient height control leads to electrode/surface collision.

Several approaches have been reported so far to overcome the fixed height problem in conventional SECM experiments. A constant-current mode combined with a vertical tip-position modulation was described in 1992.[16] A second approach based on electrochemical signaling uses convective effects when the microelectrode is moved at high speed perpendicular to the sample surface.[17] However, neither method provides current independent information on the tip-to-sample distance. A separation of the electrochemical and topographical signals was realized by the integration of the shear-force mode used in SNOM[18] into SECM.[19] A fiber-shaped microelectrode is vibrated laterally at its resonant frequency. An optical detection system with a laser, a split photodiode, and a locked-in amplifier is used to detect the damping of the vibration amplitude of the microelectrode in the near-field regime of the sample surface as a result of hydrodynamic effects. This technique was successfully applied for surface modification,[20] for positioning of nonamperometric tips,[21] and the investigation of neurophysiological processes.[22] Apart from the optical detection, a tuning-fork resonance-detection system[23] was used for current independent positioning of a fiber-shaped electrode.[24] Besides the experimental difficulties in aligning the setup with nanometer electrodes in a liquid, horizontal vibrating of the tip may affect the Faraday current to an extent, which is no longer negligible when nanoelectrodes are used.

An alternative approach to improve the resolution of SECM and to obtain highly resolved topographic information was recently published.[25,26] A first combination of electrochemical and contact-mode imaging in air was shown to be able to map the pores of a track-etched porous membrane, hydrated with an electroactive species in solution. A platinized AFM cantilever was scanned over the membrane, and electrochemistry at the apex of the tip was only achieved over hydrated pores, where the contact area between the tip and the solution determined the lateral resolution of the electrochemical signal.[25] As a result of the fact that the insulating coating is applied manually by a painting procedure, the metallized cantilever itself could not be insulated.[27] The same group demonstrated an alternative approach for expanding the application for investigations in the liquid phase.[26] A microelectrode designed like a cantilever was fabricated by etching and flattening of a platinum wire, which was insulated with an electrophoretically deposited paint,[28] thus providing an electroactive area at the very end of the tip. The flattened part of the microelectrode is used as a force sensor, and the conically shaped noninsulated tip of the electrode simultaneously provides the laterally resolved electrochemical information. Again, contact-mode imaging was carried out to investigate track-etched membranes. Furthermore, the dissolution process of a potassium ferrocyanide crystal was monitored. This approach is the first example of combined SECM−AFM imaging in liquid; however, as long as the images are recorded simultaneously in the contact mode, this system will suffer from limitations with respect to the investigable samples because of the direct contact of the exposed electroactive area to the sample surface. Thus, conducting samples, such as metal surfaces or semiconductors, may not be investigated easily using the contact mode of AFM because of short circuiting. Very recently, the same group succeeded in noncontact electrochemical imaging of a 10-μm platinum electrode with combined electrochemical atomic force microscopy based on microelectrodes designed like cantilevers.[29] Two different modes were applied. In the first mode, the topography is recorded, and after disengaging the feedback loop of the AFM, the tip is retracted from the surface using the stepper motor from the AFM, and the electrochemical image is recorded. Alternatively, the lift-mode capabilities of the instrument are utilized. In this mode, the topography of the surface is scanned in a line scan, and then the tip rescans the line at a fixed height above the surface for

(12) Nagahara, L. A.; Thundat, T.; Lindsay, S. M. *Rev. Sci. Instrum.* **1989**, *60*, 3128.
(13) Penner, R. M.; Heben, M. J.; Longin, T. L.; Lewis, N. S. *Science* **1990**, *250*, 1118.
(14) Shao, Y.; Mirkin, M. V.; Fish, G.; Kokotov, S.; Palanker, D.; Lewis, A. *Anal. Chem.* **1997**, *69*, 1627.
(15) (a) Fan, F. R. F.; Bard, A. J. *Science* **1995**, *267*, 871. (b) Fan, F. R. F.; Kwak, J.; Bard, A. J. *J. Am. Chem. Soc.* **1996**, *118*, 6996.
(16) (a) Wipf, D. O.; Bard, A. J. *Anal. Chem.* **1992**, *64*, 1362. (b) Wipf, D. O.; Bard, A. J.; Tallman, D. E. *Anal. Chem.* **1993**, *65*, 1373.
(17) Borgwarth, K.; Ebling, D. G.; Heinze, *J. Ber. Bunsen-Ges. Phys. Chem.* **1994**, *98*, 1317.
(18) Betzig, E.; Finn, P. L.; Weiner, J. S. *Appl. Phys. Lett.* **1992**, *60*, 2484.
(19) Ludwig, M.; Kranz, C.; Schuhmann, W.; Gaub, H. E. *Rev. Sci. Instrum.* **1995**, *66*, 2857.
(20) Kranz, C.; Schuhmann, W.; Gaub, H. E. *Adv. Mater.* **1996**, *8*, 634.
(21) Hengstenberg, A.; Kranz, C.; Schuhmann, W. *Chem. Eur. J.* **2000**, *6*, 1547.
(22) (a) Hengstenberg, A.; Dietzel, I. D.; Schuhmann, W**.** *Eur. J. Neurosci.* **1998**, *10*, 1303. (b) Hengstenberg, A.;. Blöchl A.; Dietzel, I. D.; Schuhmann, W. *Angew. Chem., Int. Ed. Engl.* **2001**, *40*, 905.
(23) (a) Brunner, R.; Hering, O.; Marti, O.; Hollrichter, O. *Appl. Phys. Lett.* **1997**, *71*, 28. (b) Hollrichter, O.; Brunner, R.; Marti, O. *Ultramicroscopy* **1998**, *71*, 143.
(24) (a) James, P. J.; Garfias-Mesias, L. F.; Moyer, P. J.; Smyrl, W. H. *J. Electrochem. Soc.* **1998**, *145*, L64. (b) Büchler, M.; Kelley, S. C.; Smyrl, W. H. *Electrochem. Solid State Lett.* **2000**, *3*, 35.
(25) (a) Jones, C. E.; Macpherson, J. V.; Barber, Z. H.; Somekh, R. E.; Unwin, P. R. *Electrochem. Commun.* **1999**, *1*, 55. (b) Jones, C. E.; Macpherson, J. V.; Unwin, P. R *J. Phys. Chem. B* **2000**, *104*, 2351.
(26) Macpherson, J. V.; Unwin, P. R. *Anal. Chem.* **2000**, *72*, 276.
(27) Macpherson, J. V.; Unwin, P. R.; Hillier, A. C.; Bard, A. J. *J. Am. Chem. Soc.* **1996**, *118*, 6445.
(28) Slevin, C. J.; Gray, N. J.; Macpherson, J. V.; Webb M. A.; Unwin, P. R. *Electrochem. Commun.* **1999**, *1*, 282.
(29) Macpherson, J. V.; Unwin, P. R. *Anal. Chem.* **2001**, *73*, 550.

recording the current. The tip fabrication process, including the etching process for sharpening the platinum wire and the reported insulation step, still does not facilitate the reproducible fabrication of geometrically well-defined microelectrodes, which is desirable for SECM experiments.

In the present paper, we discuss a novel approach applying a focused ion beam (FIB) technique to produce a microelectrode integrated in a standard AFM tip. Thus, a precisely defined absolute distance between the microelectrode and the sample surface can be obtained by micromachining. FIB is an attractive tool for various maskless processes with the capability for microfabrication metrology and highly resolved three-dimensional imaging of complex multilayer structures. The presented fabrication process allows the integration of an electroactive area to obtain electrochemical information at an exactly defined distance above of the end of the tip and the subsequent remodeling and sharpening of the original AFM tip for simultaneous high-resolution topographic imaging. Thus, SECM functionality can be integrated into any standard AFM without further major modification of the system, which is demonstrated with the simultaneous topographical and electrochemical contact mode imaging of a model grating containing conductive and nonconductive areas.

EXPERIMENTAL SECTION

Reagents and Solutions. Potassium ferrocyanide and potassium chloride were purchased from Fluka (Neu-Ulm, Germany). Aqueous ferrocyanide solutions contained 0.010−0.001 mol L^{-1} potassium ferrocyanide trihydrate $[Fe(CN)_6]^{4-}$ with 0.1 and 0.5 mol L^{-1} potassium chloride as a supporting electrolyte. All other chemicals were of analytical grade; the solvents were of HPLC quality.

Apparatus. AFM imaging was performed using a Nanoscope III atomic force microscope (Digital Instruments; Santa Barbara, CA). A scanning head providing a maximum image range of 120 × 120 μm was utilized. Silicon nitride cantilevers (length, 200 μm; nominal spring constant, 0.06 N m^{-1}) with integrated pyramidal tips (base, 4 × 4 μm^2; height, 2.86 μm) were used for reference measurements. The fluid cell was used for investigation under liquid.

For combined electrochemical and topographical measurements, the AFM was shielded by a home-built Faraday cage using the contact-mode base and fluid cell of the Nanoscope III instrument. A three-electrode setup, with a silver wire (Goodfellow, U.K.) operating as an AgQRE, a platinum wire as auxiliary electrode, and the integrated microelectrode serving as the working electrode, was used. Potential control and current measurements were carried out using a bipotentiostat PG10 (IPS-Jaissle; Münster, Germany). The signal output was directly connected to the data acquisition board of the AFM, allowing the simultaneous correlation of the electrochemical data with the topographical information. All images were recorded in contact-mode operation at 256 lines per scan.

Metal Coating of the AFM Cantilever by Sputtering. Silicon nitride cantilevers were initially RF sputter-coated (von Ardenne, LS 320 S; Dresden, Germany) with a 5-nm chromium layer (working pressure, 5 × 10^{-3} Torr; power, 172 W, under Ar pressure) to ensure good adhesion of the subsequently deposited metal layer. A gold layer having a thickness of 100−300 nm was then sputtered onto the cantilever to ensure a homogeneous metal film. Varying sputter times enable the application of different thicknesses of the gold layer. No distortion of the cantilever geometry was observed after sputtering up to 300 nm gold onto the cantilever.

Insulating of the Metal-Coated AFM Cantilever by Plasma-Enhanced Chemical Vapor Deposition (PECVD). Thin insulating and chemically inert coatings can be achieved by PECVD. A silicon nitride layer was deposited onto the metal-coated AFM cantilever at 300 °C by reacting tetrahydrosilane and ammonia at a pressure of 1 Torr and a power of 10 W (PlasmaLab 80 Plus, Oxford Instruments, Oxford, U.K.). To produce homogeneous, dense films without pinholes. the cantilever had to be tempered for at least 30 min at 300 °C. A film thickness of 700−900 nm was achieved by processing times between 30 and 40 min. To optimize the film thickness and the density of the produced films, the PECVD process was repeated several times with shorter deposition times. For achieving an 800-nm-thick film, 6 times 5 min was selected as the deposition parameter. For achieving a complete insulation of the standard Si_3N_4 cantilevers, which are originally gold-coated on the rear to improve the optical detection of the cantilever deflection in liquid, the PECVD process had to be carried out on both sides. Therefore, the cantilevers needed to be mounted on the tip side without destroying the tips while ensuring a proper heating of the cantilever. Simultaneous coating of several cantilevers is possible by this procedure.

Focused Ion Beam Cutting of the Modified AFM Cantilever. To obtain a well-defined microelectrode integrated in an AFM tip at a specific distance above the apex of the tip, a FIB technique (Micrion 2500 FIB system; Peabody, MA)was used.

The focused ion beam system is similar to that of a scanning electron microscope (SEM), with the major difference being the use of an ion beam instead of an electron beam. The ion beam is generated by a liquid-metal ion source (LMIS), and the application of a strong electrostatic field causes the emission of positively charged ions from liquid gallium, which is formed on the tip of a tungsten rod. Modern systems involve the transmission of a parallel beam between two lenses. A set of apertures is used to select the current of the beam and, hence, the beam size. Besides the imaging feature, the ion beam could also be used to remove material from the surface of a sample. Additionally, a gas can be introduced via gas needles positioned near the area being milled to increase etching rates and to minimize the redeposition of the milled material in the region surrounding the modified surface. This technique was found to be particularly suitable for the presented structural modifications of the AFM cantilever.

The FIB system operates at acceleration voltages between 15 and 50 kV with a gallium LMIS and allows the use of ion beams having currents ranging from 1 pA to 40 nA.

The cutting process includes several diametrically opposed cuttings, which are repeated several times in order obtain the demonstrated tip geometry. As a final step, redeposited material was removed from the electrically active part of the tip by a cleaning procedure using single-pass milling by FIB.

The electrical contact was provided by a flattened insulated copper wire (diam, 0.2 mm) glued with a conducting silver epoxy resin (Polytec; Waldbronn, Germany) to a small exposed area of the gold layer at the end of the cantilever mount. To ensure that

(a) (b) (c)

Figure 1. Modification of a standard AFM cantilever with a gold layer (RF sputtering) and, subsequently, an insulating silicon nitride film (PECVD): (a) standard AFM tip before modification; (b) 100-nm gold layer and 6 times 5 min PECVD deposition, resulting in ~800 nm of Si_3N_4 forming a homogeneous layer; and (c) 100-nm gold layer and 30-min PECVD deposition, resulting in ~800 nm of Si_3N_4 showing bubble formation.

manual handling will not scratch the silicon nitride layer, the cantilever mount was additionally protected by an insulation varnish (RS Components, U.K.) applied using a fine microbrush.

Electrochemical Experiments. The electrochemical characterization of the integrated microelectrodes was performed in a two-electrode setup, with a silver/silverchloride reference electrode (Methrom AG; Herisau, Switzerland) using an NPI VA10 potentiostat (Tamm, Germany). The electrochemical setup was located in a Faraday cage. Cyclic voltammetry was performed using a personal computer equipped with a standard data-acquisition board (CIODAS 1602, PlugIn Instruments; Eichenau, Germany) and a data evaluation software programmed in Microsoft Visual Basic 3.0 (Microsoft, Redmont, WA) provided by W. Schuhmann (Institute of Analytical Chemistry, Ruhr University, Bochum, Germany).

RESULTS AND DISCUSSION

Fabrication Steps of an Integrated Microelectrode. A standard AFM cantilever (see Figure 1a) was metalized with a gold layer by sputtering, which allows the deposition of a wide range of electroactive materials in addition to gold. Gold layers having a thickness of 100−300 nm were chosen in order to achieve a well-conducting film. The insulation of the electroactive layer is one of the crucial points in the fabrication process, particularly because of the long-term stability, chemical inertness, and homogeneity of the insulating film. Dip-coating or insulation with an electrophoretic paint[28] is not feasible, because the tip must be insulated entirely. Silicon nitride is used as a standard passivation material in microfabrication processes; thus, the demand for workability in electrolyte solutions is also fulfilled. PECVD was selected as the deposition technique because of the relatively low process temperatures. Dense and well-defined insulation layers were particularly achievable when the process was repeated several times (Figure 1b). The same cumulative processing time applied in one processing step, however, can lead to bubbles on the passivation layer, which may promote cracks in the insulation (Figure 1c).

Figures 2 and 3 schematically illustrate the fabrication steps of an integrated microelectrode along with the FIB images of the milling process.

Figure 2a visualizes the cantilever after coating with the metal layer and the silicon nitride insulation. In the first step, diametrically opposed cuttings remove the insulating layer, a part of the gold layer, and parts of the original Si_3N_4 tip, as illustrated in Figure 2b. This first milling step determines the electroactive size of the microelectrode. Figure 2c depicts the AFM tip after the first FIB cutting. The same procedure was repeated in a second step at the frontal areas of the pyramidal tip after a 90° turn of the cantilever (Figure 3a). The obtained pillar-shaped tip is covered on top with gold and the insulating silicon nitride layer. By adjusting the length of the obtained pillar-shaped tip, the distance between the microelectrode and the sample surface in correlation with the electrode area can be exactly defined. This results in the possibility of acquiring both combined electrochemical information and independent topographical imaging. Additionally, as shown in the FIB image of Figure 3a, the layers of metal and silicon nitride increase the radius of the tip curvature, as compared to the original cantilever, by a factor of 20. Obviously, this tip is not suitable for high resolution AFM imaging; hence, the described milling process must be repeated again at the side and the frontal areas of the pillar to form a nonconducting, remodeled AFM tip (Figure 3b). This procedure ensures high-resolution topographical imaging and a precisely defined and constant distance between the integrated electrode and the sample surface within the working distance for electrochemical mapping. Figure 3c finally shows the integrated microelectrode after single-pass milling with FIB as a final step to remove redeposited material from the electroactive surface. This procedure provides the same effect as a macroscopic mill, flattening the surface with the ion beam and removing accumulated material resulting from previous modification steps in a unidirectional sweep. Because of the square shape of this ring microelectrode, we denominate this new configuration as a integrated frame microelectrode, as depicted schematically in Figure 4a. The outer edge length of the depicted frame microelectrode is 2.2 μm; the inner edge length is 1.9 μm. To approximate the theoretical response of the frame electrode, the geometric factors were adapted from the ring microelectrode, denominating an inner radius of 0.95 μm and an outer radius of

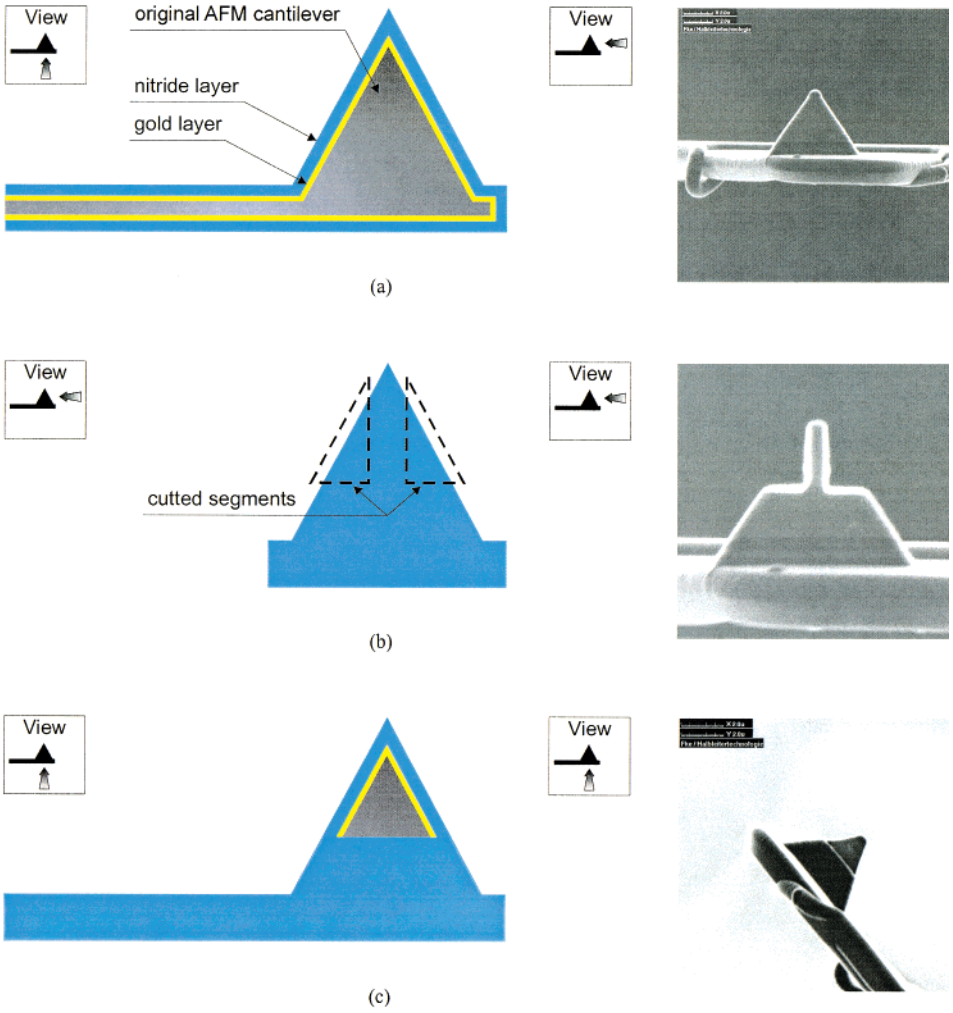

Figure 2. First set of modification steps of the coated AFM tip using a focused ion beam (FIB) technique showing (left) the schematic view of the processing step and (right) the corresponding FIB images: (a) AFM cantilever after coating with the gold layer and the silicon nitride insulation; (b) diametrically opposed FIB cuttings along the dotted lines; and (c) side view after step b.

1.1 μm (see Figure 4a). The length of the remodeled nonconducting tip was designed to be 1 μm, to correlate sufficiently with the electrode diameter. Submicroelectrodes down to 500-nm edge length have been integrated into AFM tips recently using the described procedure.

Although, in this work, a simple geometry adapted from a ring microelectrode was chosen for this first example to demonstrate the feasibility of this novel approach, accurate focusing of the ion beam allows realizing any desired geometry and shape of the integrated electrode. The achievable size of the structural features is ~25 nm and currently only limited by the diameter of the focused ion beam. Figure 4b presents a scanning electron micrograph of a microelectrode integrated in an AFM tip. As shown, the pyramidal shape of the original AFM tip determines the electrode geometry. Because more gold is deposited at the edges of the pyramid, a pillow-shaped frame geometry of the electroactive area is obtained.

Electrochemical Characterization of the Integrated Frame Microelectrode. Linear-sweep voltammetry in 0.01 and 0.005 mol L^{-1} $[Fe(CN)_6]^{4-}$ with 0.1 mol L^{-1} and 0.5 mol L^{-1} potassium chloride, respectively, as supporting electrolyte was employed to determine the insulation quality of the silicon nitride layer. Although special care was taken during the manual handling of the modified cantilevers, occasional scratching of the silicon nitride layer could not be avoided. Hence, to prevent leakage currents, the cantilever mounts were additionally protected by an insulation varnish applied using a fine microbrush. Figure 5a shows the cyclic voltammogram of an insulated AFM tip (100-nm gold layer, ~800 nm Si_3N_4 layer) without further insulation of the mount prior to FIB cutting. Figure 5b depicts a similar measurement of a mount (100-nm gold layer, ~800 nm Si_3N_4 layer), prior to FIB cutting, treated additionally with insulating varnish. Hence, by estimating the diffusion controlled current with $i_\infty = 0.02$ nA and assuming hemispherical diffusion to potential pinholes, an exposed area of ~8 nm^2 can be estimated with a diffusion coefficient for $[Fe(CN)_6]^{4-}$ of 6.7×10^{-6} cm^2 s^{-1}, as retrieved from literature.[30] An additional insulation of the mount results in a well-coated cantilever, thus demonstrating that the cantilever and the tip are entirely covered with silicon nitride. Linear-sweep voltammograms were recorded without further cleaning steps of the electrode area.

Although the shape of the integrated microelectrode is that of a square-frame microelectrode, the theoretical description of ring

(30) Kwak, J.; Bard, A. J. *Anal. Chem.* **1989**, *61*, 1221.

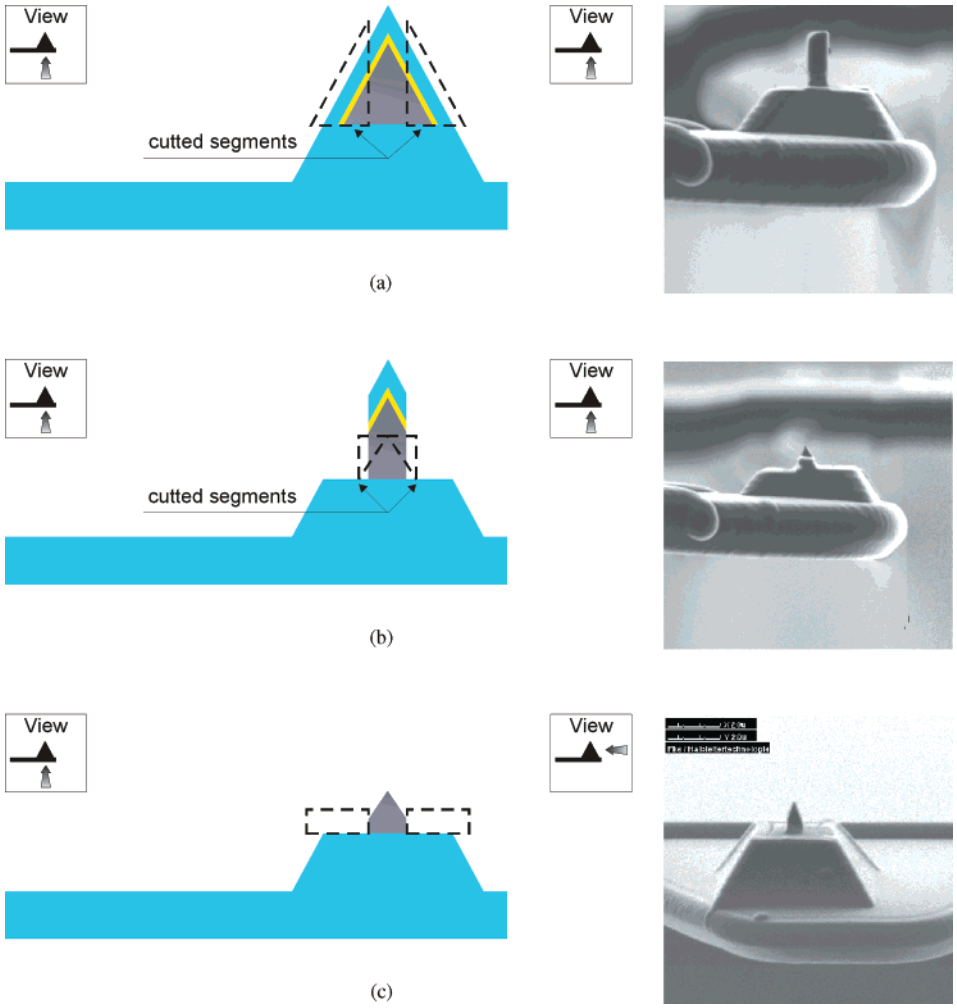

Figure 3. Second set of modification steps of the coated AFM tip uisng a focused ion beam (FIB) technique after steps 2a−c showing (left) the schematic view of the processing step and (right) the corresponding FIB images: (a) repetition of the diametrically opposed FIB cuttings of step 2b along the dotted lines after turning the cantilever by 90°, creating a free-standing square pillar; (b) remodeling of the nonconductive AFM tip by FIB cuttings along the dotted lines on all four sides of the square pillar; and (c) FIB image of the final integrated frame microelectrode (edge length, 2.2 μm) after "single pass milling" along the dotted lines for removal of redeposited material from the electroactive surface.

microelectrodes was utilized to characterize the electrochemical behavior of the tip because of the lack of a comprehensive theoretical description for square-frame electrode geometries. The steady-state diffusion current of a ring microelelectrode can be described by the following equation[31,32]

$$I_d = nFDc^*l_0 \qquad (1)$$

with

$$l_0 = \frac{\pi^2(a+b)}{\ln[16(a+b)/(b-a)]} \qquad (2)$$

D and c^* represent the diffusion coefficient and the concentration of the redox species, F stands for the Faraday's constant, n is the number of turned-over electrons, a is the inner ring radius and b is the outer ring radius. This equation is valid for a ratio of the inner to the outer radius > 0.91. For any ring microelectrode with a different thickness, the steady-state current is given by

$$l_0 = \frac{\pi^2(a+b)}{\ln[32a/(b-a) + \exp(\pi^2/4)]} \qquad (3)$$

Thus, the theoretical steady-state current for the oxidation of $[Fe(CN)_6]^{4-}$ with $n = 1$ for the cyclic voltammogram of the frame microelectrode shown in Figure 5c (inner radius, 0.6 μm; outer radius, 0.75 μm; ratio a/b = 0.80) is calculated to be 1.4 nA in a 0.01 mol L^{-1} $[Fe(CN)_6]^{4-}$ solution having a diffusion coefficient of 6.7×10^{-6} cm^2 s^{-1}. Taking the expression for any ratio of the radii, the calculated diffusion-controlled current has nearly the same value. As can be derived from Figure 5, the experimentally obtained value is about 30 % smaller than the calculated current, which may be explained by impurities and geometrical effects due to the electrode shape. Milled material may still block minor parts of the electroactive area as long as no further cleaning procedures have been applied. However, this effect is considered minor to the frame geometry of the electrode, which probably leads to a change of the steady-state current due to edge effects, as

(31) Smythe W. R. *J. Appl. Phys.* **1951**, *22* 1499.
(32) Szabo, A. J. *J. Phys. Chem.* **1987**, *91*, 3108.

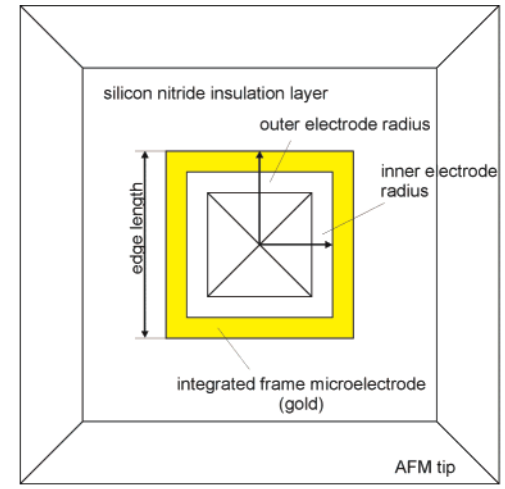

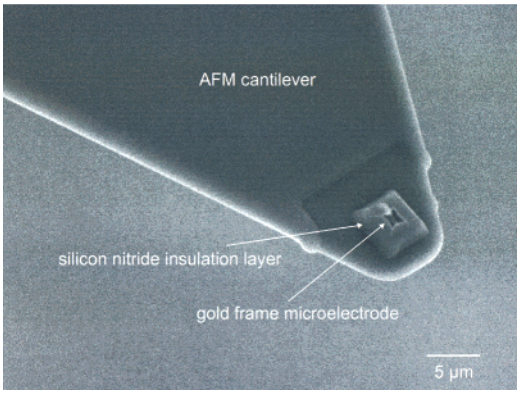

Figure 4. (a) Schematic top view describing the geometric factors of the frame microelectrode adapted from the theory of the ring microelectrode; (b) scanning electron micrograph of an integrated frame microelectrode having an edge length of 1.5 μm.

compared to a conventional ring microelectrode. This issue is the subject of ongoing theoretical investigations. A total number of 5 prototypes of integrated microelectrodes having an outer edge length of 1.5 μm have been manufactured. These showed a variation of the steady-state current within 10%.

Although the steady-state current is smaller, a similar behavior, as compared to a ring microelectrode, is evident. These results corroborate the principal functionality of the presented integrated system.

AFM Imaging with FIB-Modified Cantilevers. A major prerequisite for simultaneous electrochemical and topographical imaging is the quality and stability of the remodeled AFM tip. Hence, at different fabrication steps, contact-mode AFM images in air and in fluid were recorded, confirming that the remodeled tips with a curvature similar to the initial tips provide comparable topographic imaging quality. Micromachined gold gratings on gallium arsenide with a periodicity of 4.3 μm and a height of 0.2 μm were used as the model that is shown in Figures 6 and 7.

First investigations aimed at the feasibility of using the modified cantilevers as force sensors. Although up to 1 μm of material (gold, silicon nitride) was deposited on the flexible cantilevers, only <1% of the modified cantilevers showed undesired bending, for a total amount of >50 modified cantilevers.

Figure 6 shows an AFM image of a gold grating with a periodicity of 4.3 μm and a height of 0.2 μm recorded in 0.5 mol

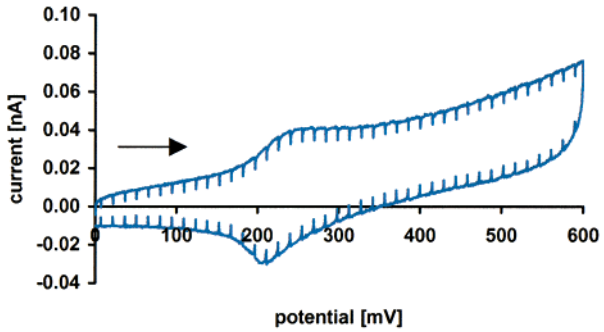

(a)

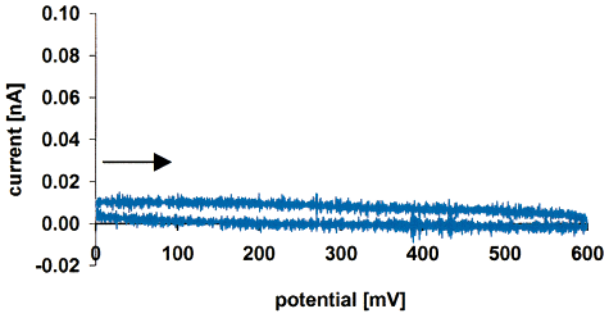

(b)

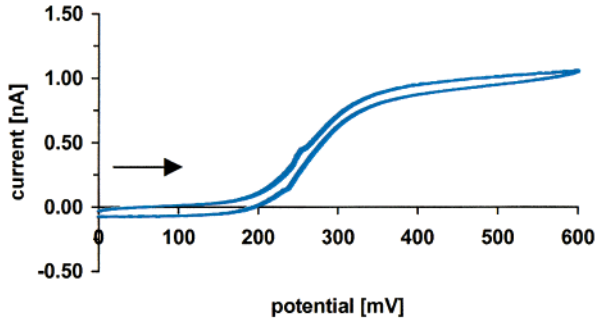

(c)

Figure 5. (a) Cyclic voltammogram recorded at a scan rate of 100 mV/s for the oxidation of 0.01 mol L^{-1} $[Fe(CN)_6]^{4-}$ in 0.1 mol L^{-1} KCl at a gold-coated and subsequently Si_3N_4-insulated AFM cantilever prior to FIB cutting; (b) cyclic voltammogram recorded at a modified AFM tip prior to FIB cutting, treated additionally with insulating varnish, having the same parameters as (a); and (c) cyclic voltammogram recorded at a scan rate of 20 mV/s for the oxidation of 0.01 mol L^{-1} $[Fe(CN)6]^{4-}$ in 0.5 mol L^{-1} KCl at an integrated frame microelectrode having an inner radius of 0.6 μm and an outer radius of 0.75 μm. Arrows indicate the scan direction.

L^{-1} electrolyte solution using a nonmodified tip. Because the periodicity of the grating is comparable to the dimensions of the integrated frame microelectrode used for the simultaneously recorded topographical and electrochemical image, this example was chosen to investigate the imaging capability of the combined tip.

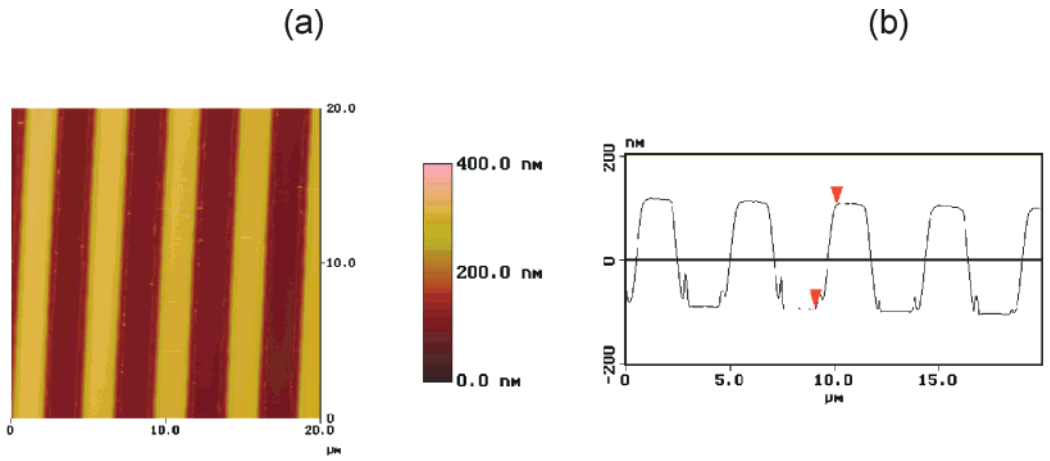

Figure 6. Contact-mode AFM image of a micromachined gold grating on a gallium arsenide substrate having a periodicity of 4.3 μm and a height of 0.2 μm, recorded using a nonmodified AFM tip in 0.5 mol L^{-1} KCl solution. Scan parameters: scan area, 20 $\times$ 20 μm; scan rate, 3 Hz. The tip was scanned from left to right and top to bottom. Surface plot and (b) height profile.

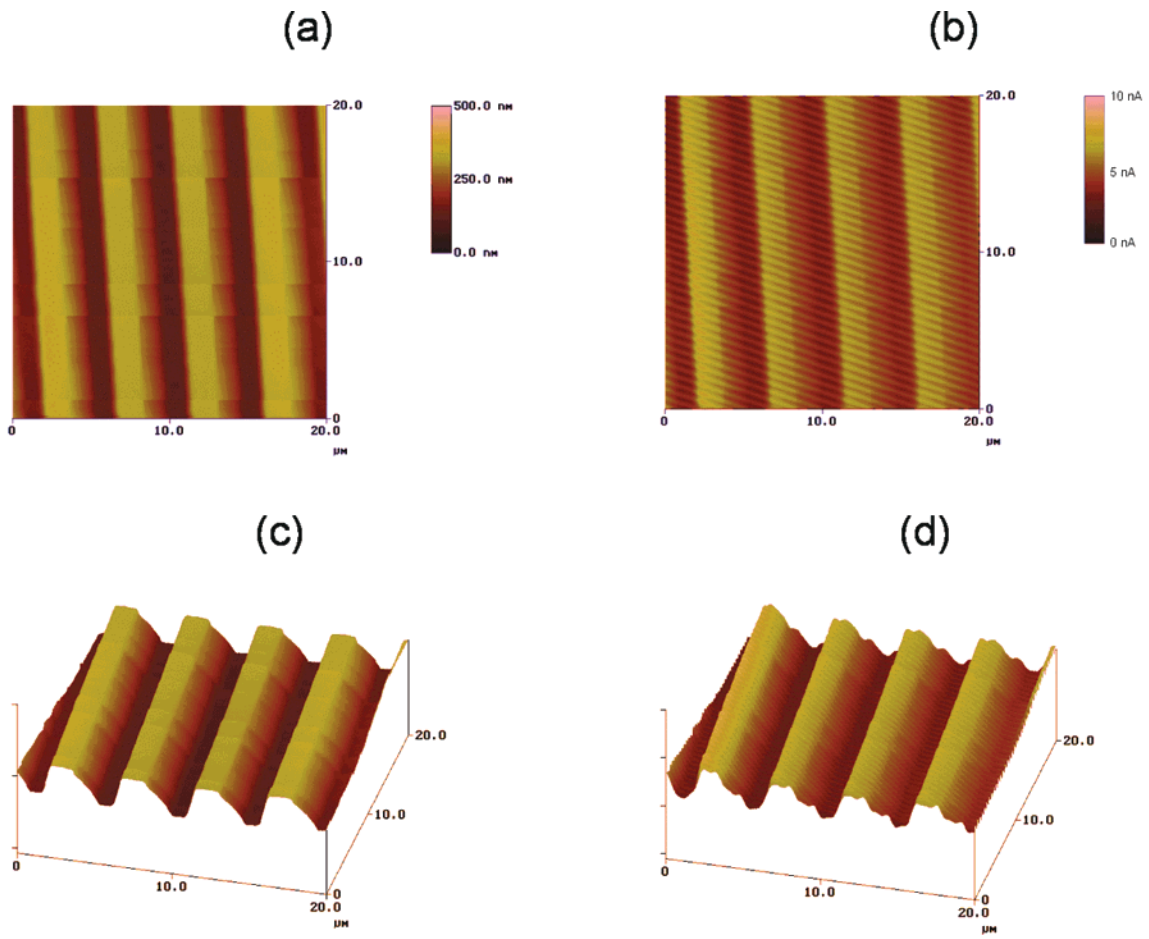

Figure 7. Simultaneously recorded height and current images of the model gold grating in 0.01 mol L^{-1} $[Fe(CN)6]^{4-}$ in 0.5 mol L^{-1} KCl. The integrated frame microelectrode had an edge length of 1.5 μm and a reshaped tip height of 700 nm. The limiting current in bulk solution was 1.5 nA. Scan parameters: scan area, 20 $\times$ 20 μm; scan rate, 2 Hz. The tip was scanned from left to right and top to bottom: (a) top view of AFM image; (b) top view of simultaneously recorded current image (the tip was held at a potential of + 0.6 V vs AgQRE); (c) surface plot of (a); and (d) surface plot of (b).

Figure 7a shows the topographical image of the model grating recorded using an integrated tip (edge length of the integrated electrode, 1.5 μm; remodeled tip height, 0.7 μm) in liquid. The quality of the image and the height of the grating agree well with Figure 6, although one side of the gold grating appears somehow leveled. This indicates that the reshaped tip is asymmetrical, which can be avoided in the future during the fabrication procedure. Furthermore, the step within the initial tip pyramid due to the remodeled AFM tip contributes to a distortion of the surface feature edges. However, as can be clearly seen, no significant loss of the imaging quality is observable. Figure 7b shows the simultaneously recorded current image of the gold grating,

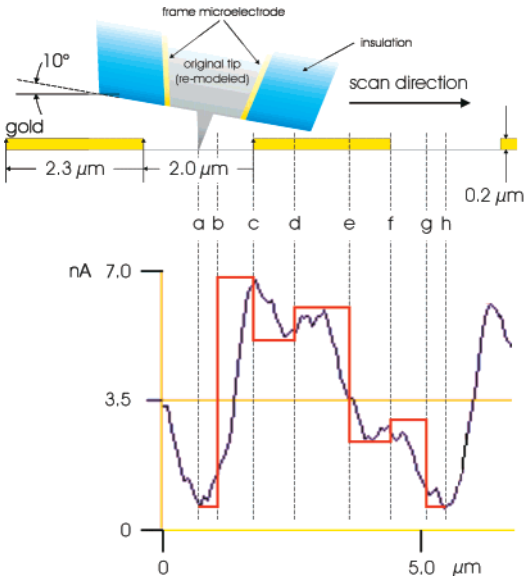

Figure 8. Schematic description of the current profile scanning (events a−h) showing the current profile recorded using the integrated frame electrode (edge length, 1.5 μm) (blue line) and the expected current profile (red line). The recorded current profile is extracted from the electrochemical image shown in Figure 7. The proportions of the schematic modified tip and the imaged surface features correspond to the real dimensions.

reproducing the periodicity of the gold stripes. The current image corresponds well to the topographical image and demonstrates the feasibility of integrating SECM functionality into a commercial AFM tip.

The periodicity of the conducting/nonconducting sections provided by the electrochemical image corresponds well to the topographical image of the gold grating on the GaAs substrate, as can be derived from Figure 7a−d. However, the electrochemical image in Figure 7d reveals that the profile of the conducting sections (gold lines) is image-broadened and not rectangular. A detailed explanation of this effect is given in Figure 8.

Figure 8 schematically visualizes the scanning procedure, including the proportions of the modified AFM tip and the surface structures scaled to real dimensions. The red line qualitatively interprets the expected relative behavior of the current when moving the integrated electrode form a to h. As can be seen, the dimensions of the integrated-frame microelectrode are within the same scale as the surface features. The reshaped nonconducting tip defines the distance of the integrated electrode to the sample surface to be 700 nm, which corresponds to the radius of the integrated frame microelectrode. Because the diameter of the integrated frame microelectrode corresponds almost to the distance between two conducting features on the surface, part of the electrode is already located above the gold line when scanning the tip from a to b. Thus, the current rises, although the reshaped AFM tip is still scanning across the nonconducting GaAs substrate. The measured current is higher than at d, because the distance of the part of the electrode above the gold strip is only ~500 nm. Scanning from b to c, the current increases until the AFM tip reaches c and follows the height of the gold strip. Thus, the current drops as a result of the enlarged distance (~700 nm) of the electrode from the gold surface at c. Moving to d, the whole active area of the integrated frame microelectrode is located above the gold strip, and the current rises again. When the AFM tip approaches e, part of the electrode is already located above the next GaAs section. As a result of the experimental setup of the Nanoscope III, the AFM cantilever is mounted at an angle of ~10° to the sample surface. Thus, the part of the electrode left to the reshaped AFM tip is located in a larger distance to the surface. This explains the asymmetrical electrochemical image of the conducting feature. Because part of the electrode remaining above the gold surface is farther away than at c and part of the electrode is already above the nonconducting substrate, the measured current at f is lower. Moving to g, the current drops again as the electrode surface above the nonconducting substrate is steadily increasing. At h, the whole electrode surface is located above the GaAs substrate, showing the same current as a. Therefore, the electrochemically imaged gold strip appears broadened and asymmetric.

This example clearly demonstrates the feasibility of this novel approach and simultaneously reveals the limitations in resolution in this particular case, where the height and size of the imaged features correspond to the size of the integrated electrode and the distance of the electrode, to the sample surface. Consequently, an improved electrochemical image of the surface features can be obtained by (i) decreasing the electrode diameter (nanoelectrodes), (ii) a smaller size of the entire tip configuration and reduced thickness of the insulating layer, and (iii) less tilt of the probing tip.

CONCLUSIONS

We present a novel approach that enables the first integration of a microelectrode into an AFM tip using micromachining techniques.

For the first time, this development enables positioning the electroactive area at a precisely defined and deliberately chosen distance from the very end of a scanning probe tip. This absolute positioning of the electrode presents an alternative to the indirect determination of the distance between the electrode and the sample surface, which is usually applied to control the position of the electrode in a scanning experiment. Thus, a complete separation of the topographical information and the electrochemical signal is possible. Furthermore, a gain in imaging speed can be predicted by the potential realization of multitip or multielectrode configurations.

On the basis of the opportunity to exactly correlate the distance of the electroactive area to the sample surface by adapting the length of the topographical probe with a micromachining technique like FIB, an optimized and defined working distance is ensured without theoretical fitting of current/distance approach curves.

As an example, a simultaneously recorded topographical and electrochemical image of a gold grating on a gallium arsenide substrate is presented and demonstrates the feasibility of this novel approach. Smaller integrated electrodes and different electrode geometries, as currently fabricated, will further improve the imaging quality.

This design is not limited to amperometric electrodes but can also be extended to potentiometric electrodes or integrated electrochemical sensors, which are particularly difficult to position

at a defined distance above a sample surface. Furthermore, the presented technique is a novel promising step toward electrochemical imaging with nanoelectrodes.

ACKNOWLEDGMENT

C. Kranz acknowledges financial support from the Deutsche Forschungsgemeinschaft (DFG) under Research Grant KR1797/1-1. B. Mizaikoff thanks the Austrian Science Foundation (FWF) for support within project P14122-CHE. The authors thank Prof. E. Gornik (Institut für Festkörperelektronik, TU-Wien) and his staff for the use of the cleanroom facilities.

Received for review September 13, 2000. Accepted March 14, 2001.

AC001099V